Reduced diffusion and perfusion in bevacizumab-induced diffusion restricted necrosis versus brain tumor hypercellularity

Peter S LaViolette[1], Elizabeth Cochran[2], Alex D Cohen[3], Mona Al-Gizawiy[1], Jennifer Connelley[4], Scott D Rand[1], Mark G Malkin[4], and Kathleen M Schmainda[1]
[1]Radiology, Medical College of Wisconsin, Milwaukee, WI, United States, [2]Pathology, Medical College of Wisconsin, Milwaukee, WI, United States, [3]Biophysics, Medical College of Wisconsin, Milwaukee, WI, United States, [4]Neurology, Medical College of Wisconsin, Milwaukee, WI, United States

INTRODUCTION Recent conflicting reports suggest that bevacizumab induced restricted diffusion as measured by decreased apparent diffusion coefficient (ADC) in regions suspicious for brain tumor infiltration, are both the result of neoplastic hypercellularity[1,2] and necrosis with restricted diffusion[3,4]. This study compares the ADC and relative cerebral blood volume (rCBV) MRI values within regions of restricted diffusion containing both hypercellularity and neighboring necrosis in a patient ex-vivo. **METHODS** *Patient Population* One patient with infiltrative high-grade glioma, underwent a biopsy followed by radiation, chemotherapy[5] and eventually bevacizumab at recurrence. At autopsy, the patient was diagnosed with glioblastoma, WHO grade 4. *Imaging* Twelve days prior to death, the patient underwent MR imaging at our institution using a 1.5T GE MRI scanner (GE, Waukesha, WI). The imaging sequence consisted of a conventional pre- and post-contrast T1-weighted acquisition. Diffusion weighted images were gathered including two b-values b=0 and b=1000s/mm^2. ADC maps were then calculated from these images. Prior to DSC, a 0.05 to 0.1 mmol/kg (pre-load) dose of gadolinium (Gd) contrast agent was administered for clinical post-contrast T1-weighted imaging[6-8]. Single shot gradient-echo (GE) echo-planar imaging was used to collect images during a second 0.1 mmol/kg bolus injection of Gd contrast. An rCBV map was calculated as previously published and standardized[9,10]. *Histology Processing* A brain only autopsy was performed on the patient. The brain was fixed in formalin and then sliced axially giving careful attention to the sagittal and coronal orientation to best slice in the same axial plane as the most recent MRI (Figure 1). Samples were taken from the brain on multiple slices. Each sample was H&E stained to reveal cell nuclei and processed with VEGF immunohistochemistry to determine regions expressing VEGF. Each slide was photographed at 10x across the entire sample using a motorized microscope stage and Nikon Instruments software (Melville, NY). Each photo was processed individually and then stitched together with all other photos using custom software written in Matlab (Mathworks, Natick, MA). The process began with a white background correction followed by a contrast optimization and segmentation of cell nuclei. One sample contained both radiation necrosis and hypercellularity within a region of decreased ADC on the MRI. For the purpose of this study, this sample was extensively studied. *Precise Histology to MRI Correlation* Custom Matlab software previously developed to precisely relate histology to the MRI (HistToMRI Toolbox)[11] was used to compare the histology and MRI findings. The brain sample of interest was co-registered manually to a single high resolution SPGR slice best representing the histology using photographs taken at the time of histology sampling. All other imaging, both ADC and histological, was co-registered and resampled to the matrix size of this SPGR image. The toolbox was then used to define a region of interest devoid of histological artifacts (outlined in red in Figure 1 center overlaid on the histology). Histology cell counts were then determined within each voxel-sized histological equivalent for 1-to-1 comparison (method shown in Figure 1). A value of cellularity < 2.5% was applied to define a region of interest that accurately segmented necrotic portions of the sample (Figure 1, far right middle, teal outline). This necrotic ROI was then resampled to the SPGR resolution, and voxels containing greater than 50% necrosis were considered for statistical analysis. ADC and rCBV values were compared between regions of necrosis and adjacent hypercellularity. An additional ROI was generated in a region of normal white matter (WM) far from the tumor for extraction of MRI values for comparison. *Statistical Comparisons* ADC and rCBV values were compared between the three tissue segmentations: necrosis, hypercellularity, and normal WM using a one-way ANOVA. P-values < 0.0001 were considered significant. **RESULTS** ADC within diffusion restricted necrosis was lower than ADC within hypercellularity and normal WM. rCBV was highest in hypercellularity, but still higher in the necrosis than normal WM (Figure 2). Restricted diffusion necrosis also had high expression of VEGF (Figure 3). **DISCUSSION** Regions of bevacizumab-induced diffusion restricted necrosis had lower ADC and rCBV than nearby regions of tumor cellularity. This type of atypical necrosis also expresses VEGF. This information should be considered when interpreting imaging to determine treatment efficacy.

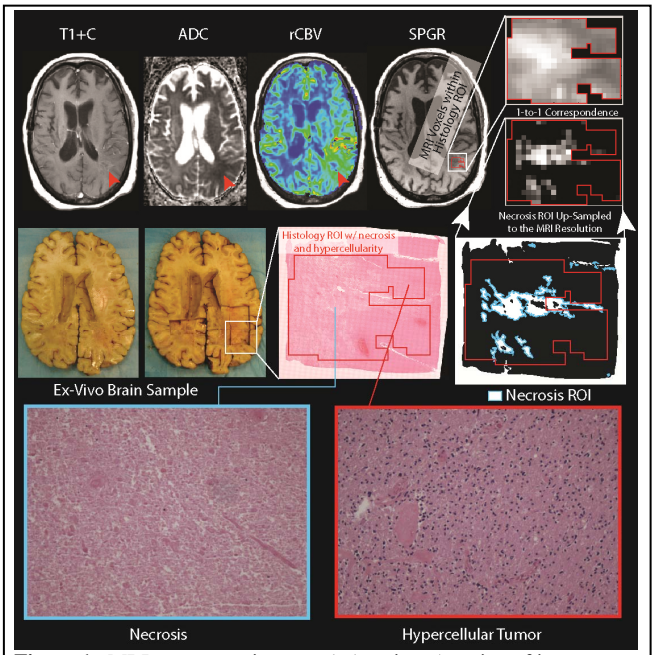

Figure 1. MRI versus ex-vivo sample location. A region of interest was created highlighting the radiation necrosis and was then up-sampled to the MRI resolution for 1to1 comparison. ADC and rCBV values from this ROI were compared to surrounding hypercellularity and a region of normal WM.

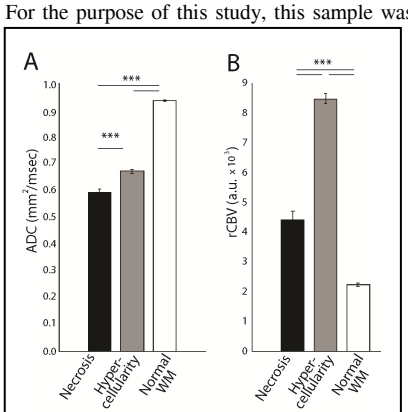

Figure 2. Bar charts demonstrating significantly different ADC and rCBV values in necrosis versus hypercellularity versus normal WM. (*** p<0.0001)

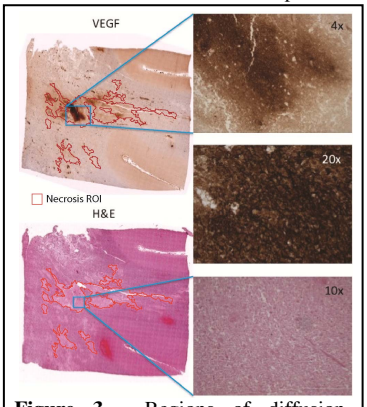

Figure 3. Regions of diffusion-restricted necrosis express VEGF.

ACKNOWLEDGEMENTS Funding: NIH/NCI R01 CA082500 and Advancing a Healthier Wisconsin, MCW Translational Brain Tumor Research Program.

REFERENCES **1.** Ellingson, B.M., *et al. J Magn Reson Imaging* **31**, 538-548. **2.** Chenevert, T.L., *et al. J Natl Cancer Inst* 92, 2029-2036 (2000). **3.** Mong, S., *et al. AJNR Am J Neuroradiol* 33, 1763-1770. **4.** Rieger, J., *et al. J Neurooncol* 99, 49-56. **5.** Stupp, R., *et al. N Engl J Med* 352, 987-996 (2005). **6.** Donahue, K.M., *et al. Magn Reson Med* 43, 845-853 (2000). **7.** Boxerman, J.L., et al. *AJNR Am J Neuroradiol* 27, 859-867 (2006). **8.** Schmainda, K.M., *et al. AJNR Am J Neuroradiol* 25, 1524-1532 (2004). **9.** Bedekar, D., et al. *Magn Reson Med* **64**, 907-913 (2010). **10.** Nyul, L.G., et al. *IEEE Trans Med Imaging* **19**, 143-150 (2000). **11.** LaViolette, P.S., *et al. Proc ISMRM, Melbourne, Australia* (2012).